Journal of Hazardous Materials 488 (2025) 137378

Contents lists available at ScienceDirect

Journal of Hazardous Materials

journal homepage: www.elsevier.com/locate/jhazmat

The spatio-temporal variability of soil microplastic distribution and erosion-induced microplastic export under extreme rainfall event using sediment fingerprinting and ^{7}Be in intensive agricultural catchment

Xiaoyan Chen [a], Zhaoyang Lu [a], Lee Heng [b], Adrian Chappell [c], Suarau Odutola Oshunsanya [a,d], Joseph Adu-Gyamfi [b], Wenxiang Liu [a,e], Hanqing Yu [a,*]

[a] Institute of Environment and Sustainable Development in Agriculture, Chinese Academy of Agricultural Sciences (CAAS), Haidian District, Beijing 100081, China
[b] International Atomic Energy Agency, Vienna, Austria
[c] School of Earth and Environmental Sciences, Cardiff University, Cardiff, UK
[d] Department of Soil Resources Management, University of Ibadan, Nigeria
[e] Chongqing Branch Institute, Changjiang River Scientific Research Institute, Chongqing 400026, China

HIGHLIGHTS

- Spatio-temporal distribution of microplastic (MP) in agro-catchment varied greatly.
- The predominance of MP $<$ 500 μm in size, with primary polymers PA, PP and PE.
- Intensive agricultural activities by policy shift greatly increased MP pollution.

GRAPHICAL ABSTRACT

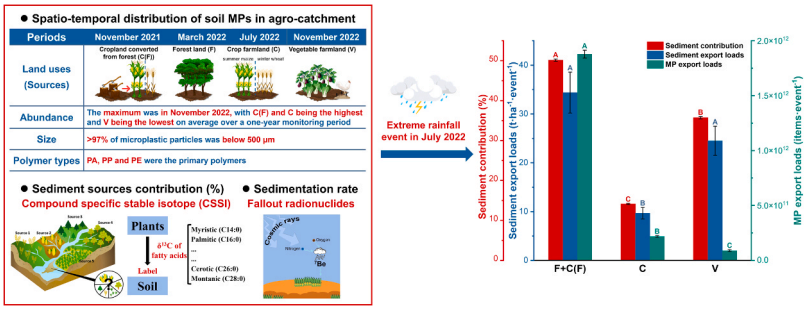

ARTICLE INFO

Keywords:
Microplastic
Spatio-temporal variability
Compound specific stable isotope (CSSI)
Berillium-7
Export loads

ABSTRACT

Intensive agricultural production and land management often lead to soil microplastics (MPs) accumulation and aggravated erosion consequently polluting water bodies. However, little is known about the occurrence and migration of soil MPs induced by soil erosion at the catchment scale. This study firstly reported the spatio-temporal variability in soil MPs distribution, and erosion-induced microplastic export loads under extreme rainfall events in an intensive agricultural catchment. The results indicated that microplastic abundance peaked in November 2022 and varied by land use types, among which cropland converted from forest (C(F)) and crop farmland (C) had the highest abundance, vegetable farmland (V) had the lowest abundance on average. Most MPs were $<$ 500 μm and the primary polymers were polyamide (PA), polypropylene (PP) and polyethylene (PE). Sediment contribution and microplastic export loads were identified using compound specific stable isotope and Berillium-7 under an extreme rainfall event. F and C(F) were merged because their $\delta^{13}C$ values were non-distinguishable and were identified as the primary sediment source (50.14 ± 0.27 %), contributing most to microplastic export loads due to land management policy shifting. Changed land uses should be the main focus

* Corresponding author.
E-mail address: yuhanqing@caas.cn (H. Yu).

https://doi.org/10.1016/j.jhazmat.2025.137378
Received 2 October 2024; Received in revised form 17 January 2025; Accepted 24 January 2025
Available online 25 January 2025
0304-3894/Crown Copyright © 2025 Published by Elsevier B.V. All rights are reserved, including those for text and data mining, AI training, and similar technologies.

for catchment erosion control and microplastic pollution prevention in intensive agriculture in China and elsewhere.

1. Introduction

Microplastics (MPs) are one of the emerging pollutants in agricultural non-point source pollution. They are defined as plastic contaminants with a particle size of less than 5 mm [1]. As chemically stable polymers, MPs have existed in the water, atmosphere and soil environment for a long time, which has resulted in adverse impacts on the environment and living organisms [2]. The soil MPs can be absorbed by crops and accumulated within the food chain thereby threatening human health [2,3]. The MPs can also cause water pollution which affects aquatic organisms and drinking water, consequently posing environmental risks [4,5]. The terrestrial soil environment is considered as the "birthplace" and the "gathering place" of MPs [6]. The microplastic abundance on land is estimated at 4–23 times that in the ocean [7]. The prevalence of MPs in sediments was also proved [8]. Eroded sediments and the associated contaminants through rainfall-driven runoff to water bodies are the main reasons for the deterioration of water quality [9,10]. The associated microplastic contaminants induced by human activities in agricultural production have caused increasingly serious agricultural non-point source pollution problems in water and soil environments, which are gaining increasing attention worldwide [2,11,12].

Land use intensification leads to greater amounts of MPs into soil as well as soil erosion, hence increasing the export loads of associated sediment [13–15]. Multiple studies showed that the microplastic abundance in intensively farmed land reached a high level and was much higher than natural lands [16–18]. For instance, a survey in the largest vegetable production base in China revealed that the microplastic abundance ranged from 310 to 5698 items•kg^{-1} while the microplastic abundance in natural woodland was 50 items•kg^{-1} in Yunnan Province [18,19]. These studies on agricultural soil MPs primarily focus on the separation and detection, distribution and hazards of soil MPs. While Wang et al. investigated 9 basins across China to estimate nano-MPs mass input from agricultural soil to riverine system via water-driven soil erosion based on the limited data using the RUSLE model [20]. There are also some studies focusing on wind erosion which caused MPs to be transported over long distance [21,22]. It is worth noting that the intensive agricultural activities, including fertilization, mechanized cultivation and harvesting, not only substantially increase the input of soil MPs but also aggravate soil erosion resulting in the sediment and MPs delivery to water system [4,14]. However, the occurrence characteristics, source and migration of MPs induced by soil erosion at the catchment scale remain unclear. Therefore, understanding spatial and temporal distribution characteristics of microplastic pollution and the export loads of land-use-based sediment and associated microplastic is imperative for conducting targeted microplastic abatement measures.

The extensively used method for identifying the contributions of sediment sources is sediment 'fingerprinting' using tracers to apportion or un-mix sediment samples into multiple sources [23]. The tracers (single component or composite) include color parameters, geochemical properties, fallout radionuclides (FRNs, e.g., caseum-137, ^{137}Cs, excess lead-210, $^{210}Pb_{ex}$ and beryllium-7, ^{7}Be) and stable isotopes [24–26]. Beryllium-7 ($t_{1/2}$ = 53.3 d), one of the cosmogenic FRNs, is also used to estimate the short-term soil redistribution and sedimentation in the catchment [27]. Recently, the compound-specific stable isotope (CSSI) technique, which utilizes the carbon-13 (δ^{13}C) stable isotope signature of fatty acids (FAs), has been widely applied to determine the contributions of land-use-based sediment sources at the catchment scale [28–30]. More recently, Lu et al. quantified sediment and associated total nitrogen and total phosphorous export loads from different land uses in an intensive agricultural catchment by combining ^{7}Be and CSSI techniques. Hence, it's achievable to quantify the export loads of sediment and the associated microplastic from different land uses [31].

The scientific question of this study is to explicate the soil microplastic distribution characteristics and identify its transportation by soil erosion into water bodies. Understanding the microplastic occurrence in different land uses coupled with quantitatively estimating the microplastic loads exported to water bodies under extreme rainfall events can serve as a basis for evaluating the ecological risks associated with the transfer of MPs accumulated in the soil to the water environment. This will also help to control the input of microplastic pollution from different sources into the water environment and consequently contribute to the prevention and control of the non-point source pollution in intensive agriculture. The objectives were to (1) clarify spatial distribution and the temporal change of microplastic abundance, size and polymer types, and (2) quantify the microplastic export loads from different land uses in an intensive agricultural catchment in North China. The joint application of ^{7}Be and CSSI will be the important technical approach to achieve the above objectives.

2. Materials and methods

2.1. Study site

The study was conducted in Jiangou catchment (40°48′00″N, 116°56′30″E) in the northeast corner of Beijing, with a total area of 13.85 km^2. Jiangou catchment is located in the major intensive grain producing areas in North China. It is a typical intensive agricultural catchment, characterized by frequent human activities and diverse land uses. Thus, the catchment is facing the risk of microplastic pollution from different land uses and water environment. The climate is characterized by a temperate semi-humid monsoon with an average annual temperature of 11.8 ℃. The 30-year average precipitation in the region is 610 mm per year, with almost 80 % of the annual rainfall occurring from June to August. The terrain has a gentle slope of 3°-10°, which gradually inclines from northwest to southeast. The streams flow out of the only outlet in the low-lying area of the catchment and into the tributary of Haihe River, which is one of the seven major water systems in China.

The distribution, area and percentage of each land use in the catchment were obtained by field surveys and ArcGIS Desktop (Release 10.2, Environmental Systems Research Institute 2018, Redlands, CA) associated with Google Earth (Fig. 1). Characteristic land use types in the catchment included forest (30 %), crop farmland (31 %), vegetable farmland (6 %), residences (13 %), rock hilly area (7 %), dairy farm (built-up areas; 0.6 %) and ponds (0.4 %). In the forests, there were White Poplar (*Populus tomentos*), Chinese pine (*Pinus tabuliformis*), Siberian Elm (*Ulmus pumila*) and Purple-leaf Plum (*Prunus cerasifera f. atropurpure*). Crop farmland comprised cropland converted from forest, where maize (*Zea mays*) was rotated with wheat (*Triticum sativum*). Vegetable farmland was used to plant onion (*Allium*), lettuce (*Lactuca sativa var. Augustana*), garlic (*Allium sativum*) and tomatoes (*Lycopersicon esculentum*). Due to the policy of "Return the Forest to Farmland" and other factors under the background that the Chinese government issued a "high standard" farmland construction (HSFC) plan of 716,667 km^2 by 2025, the percentage area of crop farmland increased by 16 % since the end of 2020 [32]. The improved farmlands possess the following critical characteristics: being level, clustered and contiguous, having perfect supporting facilities, fertile soil and strong resistance to disasters. There was about 0.8 km^2 of newly completed high-standard farmland in the catchment, of which about 0.18 km^2 was converted from forest [33]. Compound fertilizer was used for crop farmland before sowing summer

maize in April and winter wheat in September. Farmyard chicken manure from free-range chickens raised by small-scale farmers was mainly applied to vegetable farmland.

2.2. Sample collection

According to the vegetation type, field surveys in the area and our previous work [30], four primary land uses were identified as the major sediment contributors in the catchment: cropland converted from forest (C(F)), forest land (F), crop farmland (C) and vegetable farmland (V).

2.2.1. Source soil and sediment samples

Source soil and sediment samples were used for the measurement of microplastic and CSSI ($\delta^{13}C$ of Bulk C and FAs) and collected as the following procedure. The topsoil (0–2 cm) sampling of four land use types was performed in scattered sites. The sampling points were randomly selected in each sampling site with an area of about 100 m^2 in each land use. Thereafter, 15 sub-samples were randomly collected at each sampling site using a topsoil collector and evenly mixed into one composite sample. This composite sampling strategy was designed to reduce the spatial variation of FAs signatures. The number of composite samples (the number of sampling sites) for each land use was as follows: C(F) (n = 8), F (n = 22), C (n = 12), V (n = 18). The number of sampling sites was mainly based on the area of each land use. In addition, we considered the erosion potential and connectivity of each land use to mainstreams, in order to quantitatively assess the ecological risks posed by the loads of sediment and associated microplastics exported into water bodies, as reported by similar studies [28,34–36]. These spatially-integrated composite samples enable this study to obtain the real representative samples of each land use type and therefore a trade-off between the spatial variability of CSSI values and microplastic abundance and analytical costs, which are necessary to meet the research objectives.

The sediment samples had the same layer depths and number of sub-samples and were collected at the catchment outlet. A total of 32 composited sediment samples were collected. During sampling, insects, sticks, leaves, stones and other residues were removed. All samples were collected in November 2021, March 2022, July 2022 and November 2022.

2.2.2. ^{7}Be soil samples

The topsoil sampling for ^{7}Be measurement was conducted immediately after the heaviest rainfall event in July 2022. The accumulated rainfall reached 86.3 mm from July 1st to 3rd, 2022. The 24-hour rainfall amount (62.4 mm) on July 1, 2022, was considered a rainstorm because it exceeded the 50 mm threshold. Additionally, there were two periods of hourly rainfall on that day with 21.4 mm and 20.8 mm, respectively; both exceeding the 20 mm threshold typically regarded as short-term heavy rainfall.

A total of 13 ^{7}Be samples were collected from sites randomly selected at the catchment outlet on depositional mudflats. Samples were collected from the surface layer (0–2 cm) soils using a topsoil collector. In addition, three replicate sites (1 m × 1 m) were established as reference sites in a flat area, where weeds were removed regularly to prevent the interception of ^{7}Be. At all three reference sites, a total of 5 samples were collected from the surface layer (0–2 cm) soils. The soil profile sampling for determining the relaxation mass depth of ^{7}Be (h_0) was carried out at 2 mm depth increments within the 0–10 mm layer and 5 mm increments within the 10–20 mm layer [37].

2.3. Laboratory processing and analysis

2.3.1. MPs extraction, quantification and identification

Samples were subjected to processing and analyses to obtain information on the abundance, size, and polymer type of MPs. The collected soil from different land uses and sediment composite samples were air-dried, passed through a 2 mm sieve and thoroughly mixed. Weigh a portion of the well-mixed sample for subsequent extraction and analysis

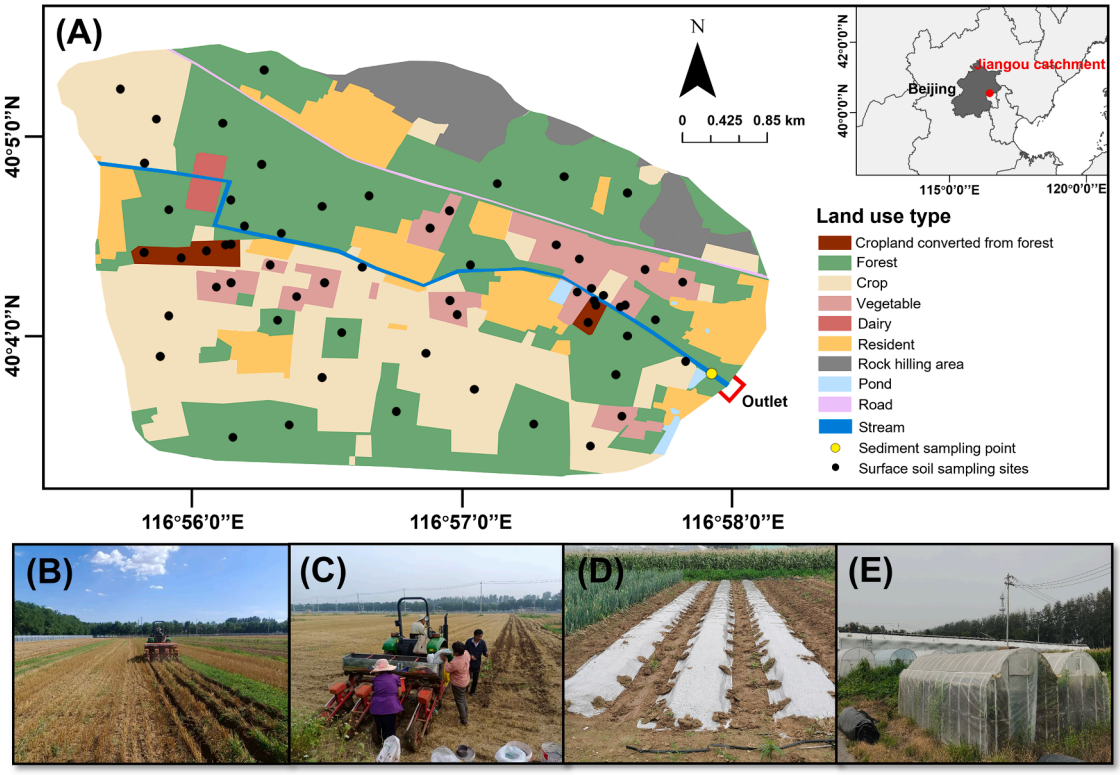

Fig. 1. Location of the Jiangou catchment with different land uses (A) and potential microplastic sources in the catchment: ploughing (B), sowing and fertilizing (C), mulch film (D) and greenhouse (E).

experiments. The density-flotation separation method with saturated zinc chloride solution ($ZnCl_2$) solution was used to extract MPs from samples [17,38]. The weighted samples were mixed with filtered saturated $ZnCl_2$ solution and the mixture was stirred thoroughly for 30 minutes. After leaving to settle for 12 hours, the supernatant liquid containing MPs was separated from the sample into a clean beaker. The 30 % (vol/vol) H_2O_2 solution was added into the beaker and digested the liquid in a 40 ℃ water bath for 2 hours to eliminate the interference of organic matter. Thereafter, the Nile red dye was added to the solution for the staining of MPs. Then the solution was vacuum filtered and the MPs were captured on the filter membrane. To ensure the uniform distribution of microplastics on the filter membrane, we implemented specific operational steps. Firstly, to guarantee the even suspension of microplastics in the solution. We continuously stirred the solution with a glass rod, facilitating a more uniform collection of particles on the whole filter membrane. Secondly, as the filtration process came to an end, a small amount of water was cautiously and slowly added along the inner wall of the filter cup, which enabled the collection of particles adhering to the cup wall onto the filter membrane without disturbing the particles on the surface of the filter membrane. The filter membrane was transferred to a clean glass Petri dish for further analysis. There were three replicates for each sample.

As the count of all particles on the filter membrane surface would be extremely time-consuming and costly, only a portion of sites on each membrane were examined to optimize the observation process, as other studies have documented [39–45]. We selected representative sites on the filter membrane for analysis by referring to the above quantitative methods for MPs. These representative sites on each filter membrane were selected using an "N" shaped pattern [40,45]. All particles of each replicate sample from selected sites were counted, analyzed and identified. Fluorescent microscopy (LEICA, LAS X, Germany) was used to photograph and store the pictures of the filter membrane segments containing the collected MPs in both fluorescent and normal white light modes. By comparing the fluorescence and white light microscopic images and adjusting the threshold and detection limits of the fluorescent microscopy images, the information about the quantity (counting) and size of MPs was obtained using (Image J) software. The detailed method of calculating microplastic abundance in the samples was presented in the supplementary materials (Text S1). The infrared spectra of suspicious microplastic particles were measured using a Fourier transform infrared microscope (Bruker Optik GmbH, LUMOS, Germany) in attenuated total reflectance mode (FTIR-ATR). The obtained spectra were compared with the standard spectra retrieved by the infrared spectral library (Bruker, Germany) using OPUS software with a similarity threshold of 70 % [17,38,46–48].

2.3.2. Bulk C $\delta^{13}C$

The source soil and sediment samples were processed to measure the Bulk C $\delta^{13}C$ following Gibbs' protocol [49]. The dried samples were acidified with 10 % hydrochloric acid (HCl) solution to remove inorganic carbonates. Then the total organic carbon ($\%C_{org}$) and $\delta^{13}C$ of the bulk soil were analyzed by the elemental analyzer (Flash EA1112, ThermoFisher., CA, USA) coupled to an isotope ratio mass spectrometer (Isoprime 100, Elementar Ltd., Frankfurt, Germany). The $\delta^{13}C$ was calculated by expressing the measured ratios (R_{sample}) against an international standard Vienna Peedee Belemnite (VPDB) standard ($R_{standard}$):

$$\delta^{13}C\ (‰) = \left(\frac{R_{sample}}{R_{standard}} - 1\right) \times 1000 \quad (1)$$

2.3.3. Extraction and determination of fatty acids

FAs were extracted, fractionated and methylated to determine the $\delta^{13}C$ according to a standard approach [50]. The sample was extracted with dichloromethane, saponified and then adjusted to acidity. After removing impurity with anhydrous sodium sulfate (Na_2SO4), fatty acid methyl esters (FAMEs) were obtained by adding methanol solution of boron trifluoride (BF_3) and then dissolved in n-hexane solution. GC-IRMS (Trace GC Ultra, ThermoFisher., CA, USA; Delta V Advantage, ThermoFisher, Bremen, Germany) was used to analyze carbon isotope composition ($\delta^{13}C$ values) of individual FAMEs. The methanol employed for digestion was analyzed for $\delta^{13}C$ to amend FAMEs isotope values for inclusion of methyl compound as follows:

$$\delta^{13}C_{FA} = \frac{\delta^{13}C_{FAME} - (1 - X)\,\delta^{13}C_{Methanol}}{X} \quad (2)$$

where X is the ratio of carbon atoms in the FA to the carbon atoms in the corresponding FAME. The analytical precision is estimated at 0.2 ‰.

2.3.4. ^{7}Be activity

For the measurement of the ^{7}Be activity ($Bq{\cdot}kg^{-1}$), collected samples were passed through a 2 mm sieve. Then the measurement was conducted by using a broad-energy hyper pure coaxial Ge (HPGe) detector with a relative detection efficiency of 50.9 % (BE5030; Canberra Industries Inc., Meriden, CT, USA). The activity of ^{7}Be in samples was detected at 477.6 keV peak using counting time over 80,000 s in order to provide an analytical precision of ± 10 % [51].

2.4. Rainfall monitoring

A rainfall gauge (HOBO UA-003–64, Onset Computer Corp., Bourne, MA USA) was used to record daily rainfall in the Jiangou catchment from September 2021 to January 2023.

2.5. Proportion of sediment source contribution

The principle of the CSSI method is based on "land use" defined by the plants growing on that land. Plants can produce different organic compounds (e.g. FAs) that "leak" from the roots or leach from leaves into the soil, which can serve as unique "biomarkers" for different land uses and remain stable. Although the range of saturated FAs is the same, the $\delta^{13}C$ ($^{13}C/^{12}C$) values of FAs are different [50]. This unique isotopic signature is produced by the discrimination against ^{13}C by different plant types and can be measured by the $\delta^{13}C_{FA}$. For instance, the $\delta^{13}C_{FA}$ values for C4 plants are more positive, while those of C3 plants are more negative [52,53]. Based on the principle above, the tracers were pre-selected according to the following criteria: 1) the tracers should originate from terrestrial higher plants and be dispersed to the whole upper soil layer by the roots under the influence of infiltration rain; 2) they must remain conservative during their movement process through the catchment; 3) the tracers with little difference between potential sources should be excluded [23].

To estimate the contribution of multiple sources to sediments based on tracer isotopic signatures (e.g. FAs $\delta^{13}C$, etc.), Bayesian mixture models (e.g., MixSIR, SIAR and MixSIAR) were employed with biotracers such as FAs and stable isotopes [54,55]. According to existing literature and our previous study [24,28,31,56], the Bulk $\delta^{13}C$ and FAs $\delta^{13}C$ (C14:0-C28:0) were regarded as potential tracers. Based on the results of further statistical testing, the proportions of selected carbon isotopes of different land use sources in sediment mixture were determined by using MixSIAR model. The carbon isotopic proportions were converted to source soil proportions (*Source*, %) using a linear conversion equation as follows:

$$\%Source = \frac{I_n / \%C_n}{\sum_n^1 (I_n / \%C_n)} \times 100 \quad (3)$$

where I_n is the mean feasible isotopic proportion of "source n" in the mixture as estimated from isotopic values of carbon by the mixing model, and $\%C_n$ is the % carbon in the source n soil.

2.6. Export loads of microplastic under an extreme rainfall event

^{7}Be is a natural radionuclide with a half-life of only 53.3 days.^{7}Be technique has been successfully used to estimate short-term (based on rainfall events) soil sedimentation in the catchment, by comparing the ^{7}Be inventory at the catchment outlet with that of the reference sites [27]. The sedimentation rate (*SR*) at the catchment outlet was calculated according to the Profile Distribution Model (PDM) [57].

^{7}Be technique was combined with the CSSI technique (to identify sediment source contribution) and microplastic abundance of different land uses to calculate the land-use-based microplastic export loads under an extreme rainfall event. The export loads of MPs (El_{MP}) were calculated as:

$$El_{MP} = SR * C_S * \quad A_S * MP_C \tag{4}$$

where El_{MP} (items·event^{-1}) is the microplastic export loads from each land use; *SR* (t·ha^{-1}·event^{-1}) is the sedimentation rate at the outlet of the catchment; C_S is the contribution of each land use to total sediment export in the catchment (%); A_S (ha) is the area of each land use in the catchment; MP_C (items·t^{-1}) is the microplastic abundance of samples from each land use.

2.7. Quality control and statistical analysis

To minimize potential microplastic contamination, strict quality control measures were implemented. Cotton lab coats and gloves were worn during the experiments. All instruments and glassware were cleaned, rinsed with ultra-pure water, dried before the experiment, and stored in clean cabinets when not in use. All exposed vessels were covered with aluminum foil during the experiments to prevent contamination. The ultra-pure water and solutions required for the experiments (saturated $ZnCl_2$ solution and H_2O_2 solution) were passed through ultrafine filter membranes (47 mm in diameter and 0.22 μm in pore size) using a glass sand core filter and a vacuum pump. Blank experiments were repeated three times, and the detected MPs were subtracted as background value to ensure the reliability of the experimental results during the analysis process of MPs.

The abundance of microplastic in samples (items·kg^{-1}) is expressed as the number of MPs within a unit weight of dried samples [58]. Due to the constraints of the stereo microscope, the observation limit of MPs is 10 μm. The MPs size less than 10 μm were difficult to recognize and were recorded as zero. Statistical analysis was performed using SPSS 25.0 (IBM Corp., Armonk, NY, USA). ArcGIS associated with Google Earth was used for geographic mapping. Figures were produced using Origin 2022 (OriginLab Corporation, Northampton, MA, USA). One-way analysis of variance (ANOVA) followed by Duncan's test was used to analyze differences in microplastic abundance under different land uses and outlet of Jiangou catchment across all monitoring periods. Data were expressed using the mean and standard error, and the significant difference threshold was set at $p < 0.05$.

3. Results and discussion

3.1. The spatio-temporal variation of microplastic abundance

The microplastic abundance of C(F) and C was the highest and V was the lowest on average over a one-year monitoring period, ranging from 38,223 to 98,602 items•kg^{-1} (Fig. 2). The abundance of MPs detected in our study was much higher than the results in other similar studies. For example, the average microplastic abundance in cultivated land of Yunnan Province and plastic mulched agricultural fields of Xinjiang was 9800 items•kg^{-1} (sampled at 0–30 cm) and 12,598 items•kg^{-1} (sampled at 0–20 cm), respectively [59,60]. Furthermore, Zhang et al. revealed the microplastic abundance of up to 42,960 items•kg^{-1} (sampled at 0–10 cm) in the Chai River valley in southwestern China

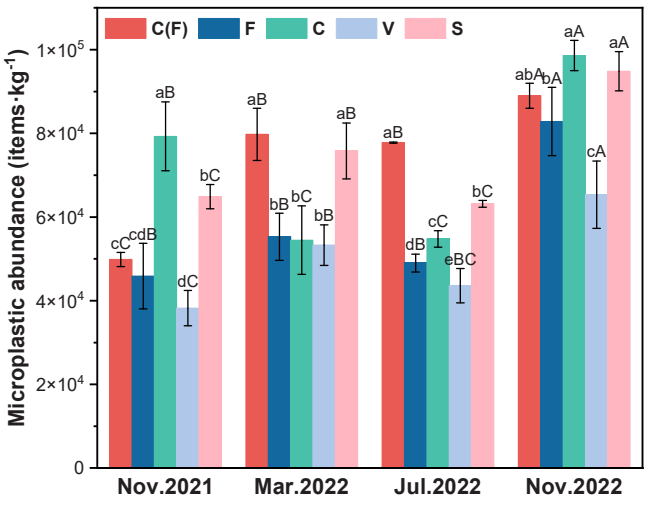

Fig. 2. The soil microplastic abundance under different land uses and outlet of Jiangou catchment which were sampled in November 2021, March 2022, July 2022 and November 2022 respectively. Note: C(F): cropland converted from forest, F: forest land, C: crop farmland, V: vegetable farmland and S: sediments at the outlet of Jiangou catchment. Different lowercase letters indicate significant differences in microplastic abundance under different land uses and outlet sediments in the same period, and different uppercase letters indicate significant differences in microplastic abundance from the same land use type and outlet sediments in different periods (Duncan analysis, $p < 0.05$).

[61]. The higher abundance of MPs (up to 98,602 items•kg^{-1}) observed in this study is very likely caused by the difference in sampling depths. Previous studies demonstrated that soil MPs were mainly concentrated in the surface layer and the microplastic abundance declined greatly with the increase of soil depth [17,38,62]. The soil samples in our study were taken at the depth of 0–2 cm, because the MPs in the surface soil tend to migrate with soil erosion and runoff [63,64], and what we need to investigate was exactly the microplastic export to the water body driven by erosion. Additionally, the 0–2 cm surface soil samples were required to quantify the microplastic export loads by CSSI and ^{7}Be techniques. Hence, it is necessary to determine the soil microplastic abundance with the same depth for consistency. Similar to our study, the research using topsoil samples (0–5 cm) also showed a high level of microplastic abundance (range of 2.2×10^4 to 6.9×10^5 items•kg^{-1}) [65].

In November 2021, the microplastic abundance of C (79,294 items•kg^{-1}) and S (64,879 items•kg^{-1}) was statistically significantly higher than that of C(F), F and V. While in March 2022, the microplastic abundances of C(F) (79,771 items•kg^{-1}) and S (75,789 items•kg^{-1}) were significantly higher than those of F, C and V. In July 2022, there were statistically significant differences in microplastic abundance between source soil and sediment in the following order: C(F) > S > C > F > V. In November 2022, the microplastic abundance of C(F) (88,986 items•kg^{-1}), C (98,602 items•kg^{-1}) and S (94,868 items•kg^{-1}) was statistically significantly higher than that of F and V ($p < 0.05$). Our results indicated that MPs were ubiquitous in the soil environment but their abundance varied in different land uses, which was attributed to human activities especially intensive agricultural practices. The risk of microplastic pollution was higher in intensively managed lands (C and C (F)) compared to less managed lands (F and V). Similarly, the microplastic pollution in croplands and pastures was more serious than in natural grasslands and forests [16,66,67].

The common feature of temporal variation of microplastic abundance was that the microplastic abundance under different land uses (C (F), F, C and V) and sediment (S) in November 2022 was significantly higher than that in the other three periods. The microplastic abundance of C(F) in November 2021 was statistically significantly lower than that

in March, July and November 2022. The microplastic abundance of F was not statistically significantly different in November 2021, and March and July 2022.

The microplastic abundance of C(F) in November 2021 was the lowest because the agriculture was still under construction. In Mar 2022, C(F) was put into full use. A series of intensive agricultural practices, including mechanical ploughing, sowing and fertilization, substantially increased the input of MPs in farmland soil [14,15]. During this process, the wide use of fertilizer, agricultural machines and relevant plastic products significantly increased the abundance of MPs by 59.99 % in our study. In particular, fertilizer application was the primary factor contributing to the microplastic pollution in agricultural soil. On one hand, fertilizer packaging bags and ropes without efficient disposal were one of the significant sources of microplastic contamination. On the other hand, the extensive application of polymer coated fertilizers led to the remaining soil MPs [68]. A survey in Japan revealed that the use of polymer-coated fertilizers in paddy fields resulted in a high concentration of microplastic up to 369 $mg \cdot kg^{-1}$ [69]. In our study, during November 2022, the microplastic abundance of C(F) increased dramatically and reached its maximum coinciding with the input of machinery work and fertilizer needed for crop harvesting and sowing. The use of plastic products and fertilization in farming activities resulted in the accumulation of soil MPs, which would enter the water environment and cause water pollution [11]. Besides, microplastic particles can be absorbed by crops and accumulated within the food chain, thereby posing a threat to human health [3].

The microplastic abundance of C in November 2022 was the highest, which was attributed to the input of machinery work and fertilizer used for crop production. However, the microplastic abundance was significantly lower in March and July compared to other seasons. For March, there was no sowing or harvesting of crops during this period. For July, the wheat harvesting and surface ploughing with sowing attract less soil disturbance compared to maize harvesting followed by deep ploughing with sowing in November. Thus, the microplastic abundance increased with increasing intensive agricultural practices on the C [14,15]. Additionally, MPs in topsoil were carried away by surface runoff and soil erosion under the extreme rainfall event in July [64,70]. Consequently, the microplastic abundance of C in March and July did not increase much, which was attributed to rainfall and lower agricultural activity intensity.

In addition, there is a relationship between the soil management practices of each land use type and microplastic abundance. The major land management in this catchment was the conversion of some forest land into cropland. Figure S1 illustrated the relationship between soil management practices and microplastic abundance before (2019) and after (2022) land management policy shift. Microplastic abundance increased from forest to crop farmland and cropland converted from forest (C+C(F)). Soil management practices and microplastic abundance are directly related as shown in Figure S1.

Unexpectedly, F was more contaminated with MPs than V. This could be attributed to the management measures in forest land, which included economic forest and planted forest. The fertilization and mechanical ploughing in economic forest raised the input of MPs into forest land soil. The largest forest land near the dairy farm in the catchment was ploughed and fertilized with cow manure in November 2022, which was responsible for the significant increase in microplastic abundance of F in November 2022. The microplastic abundance of F in other periods did not increase much because there was no big disturbance. However, there was less microplastic entering vegetable farmland since the farmers have been using farmyard chicken manure as fertilizer. The microplastic abundance of V fluctuated, which was related to the vegetable species and vegetable production. The growth cycle of vegetables was short and they were usually harvested multiple times per year, hence the vegetable farmland tended to suffer more outside interference. Consequently, the microplastic abundance of V gradually increased with time but decreased in July 2022. The reason for this decline was that MPs in topsoil were carried away by surface runoff and soil erosion especially the low-density MPs (such as PP and PE) [21,63,71]. Microplastics were expected to move upwards when the soil was saturated with water after rainfall or irrigation, and then migrate with surface soil-water loss [64,70,71]. Thus, the heavy rainfall in July 2022 promoted MPs to migrate into the river from the uplands in the catchment. The microplastic abundance of V peaked in November 2022 because of more disturbance due to the harvesting of root vegetables such as white radish.

The microplastic abundance of S was related to the microplastic abundance level of four sources and rainfall intensity. The higher the microplastic abundance of the source areas, the greater the microplastic abundance of sediment. The large difference in sediment microplastic abundance in July 2022 was attributed to the rainfall intensity and sediment connectivity. Under low-flow river conditions, sediment MPs usually accumulated, whereas under high-flow conditions, they were reduced. The flushing effect of rainfall on the riverbed resulted in a decrease of 34.86 % of the microplastic stock in the sediment, and the elimination capacity was influenced by the rainfall intensity [72]. The heaviest rain in July 2022 increased the river water velocity, which led to the migration of MPs from sediment to surface water [73,74].

3.2. The size characteristics of MPs

The microplastic sizes were classified into five categories: 10–100 μm, 100–200 μm, 200–500 μm, 500–1000 μm and 1000–5000 μm (Fig. 3). Microplastics with particle size of 10–100 μm had the highest frequency, ranging from 49.33 % to 94.38 % of the total MPs content under different land uses and outlet of Jiangou catchment. Microplastics with the size classes of 100–200 μm, 200–500 μm and 500–1000 μm accounted for 13.51–39.39 %, 4.58–15.32 % and 0.64–2.90 % of the total MPs content, respectively. Large MPs (1000–5000 μm) were absent in most samples. The results indicated that MPs smaller than 500 μm had the highest contribution (> 97 %), which was consistent with the results of agricultural areas on the eastern Qinghai-Tibetan Plateau, the largest vegetable production base in China and plateau cultivated land of Yunnan Province [19,60,75]. The dominance of MPs with small particle size was induced by natural and anthropogenic factors. Thermal oxidation, natural ultraviolet irradiation, biodegradation and other natural processes break MPs into smaller-sized particles [76]. Fertilizer application is expected to not only increase the input of MPs with small particle size, but also indirectly promote the degradation of MPs. For instance, nitrogen and phosphorus fertilizer application can accelerate the decomposition of MPs because it increased the abundance and biodiversity of microorganisms involved in microplastic degradation [77].

3.3. The polymer characteristics of MPs

Based on the FTIR-ATR analysis results, there were 12 types of microplastic polymers detected, including acrylonitrile butadiene styrene (ABS), ethylene butyl acrylate (EBA), phenolic epoxy resin (EP), polyamide (PA), polyethylene (PE), polyethylene glycol terephthalate (PET), phenol formaldehyde (PF), polyformaldehyde (POM), polypropylene (PP), polyphenylene (PPP), polystyrene (PS) and rubber. PA (12.5–85.71 %) was the primary polymer type in most samples especially in July 2022, followed by PF (9.09–50 %), PP (7.69–50 %) and PE (7.69–33.33 %). Other proportions of PET, POM and PPP in the samples were relatively small (only 16.67 % in C(F) in March 2022, only 7.69 % in V in November 2021 and only 9.09 % in V in July 2022 respectively) (Fig. 4). Fig. 5 showed the corresponding relationship between size and polymer types of MPs. Within 10–100 μm particle size, PA, PP and PE accounted for 55.26 %, 13.16 % and 13.16 % respectively. Subsequently, particle size distribution among MPs was in the order of PA (27.54 %), PE (17.39 %), PF (13.04 %) and Rubber (13.04 %) in 100–200 μm. While PA, PF and PP explained 35.29 %, 17.65 % and

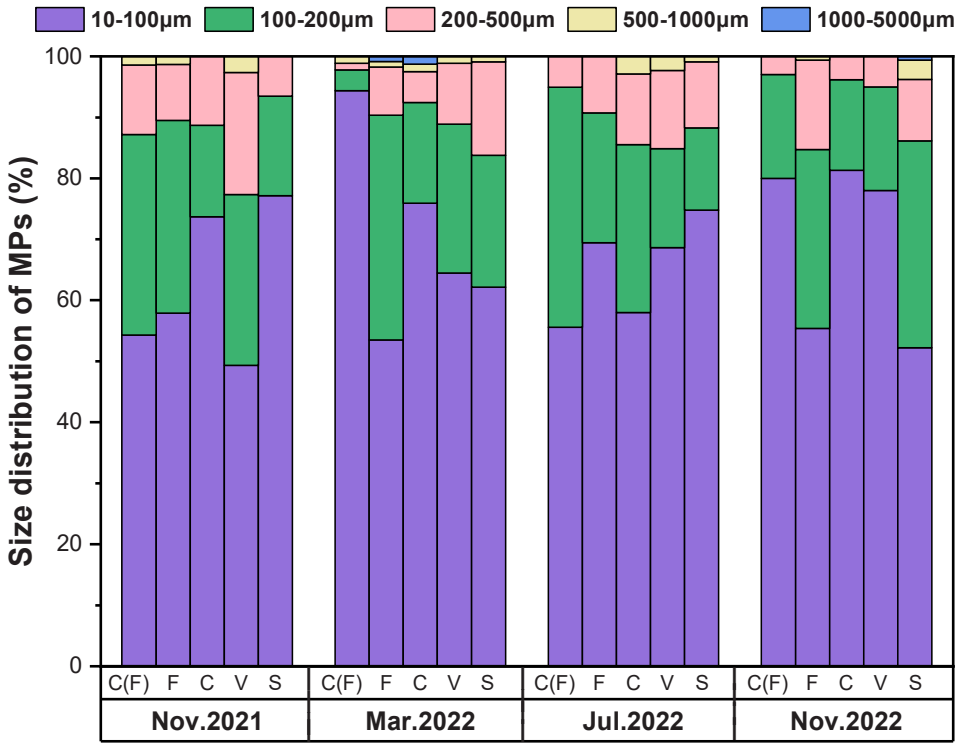

Fig. 3. The size distribution of MPs under different land uses and outlet of Jiangou catchment which were sampled in four monitoring periods.

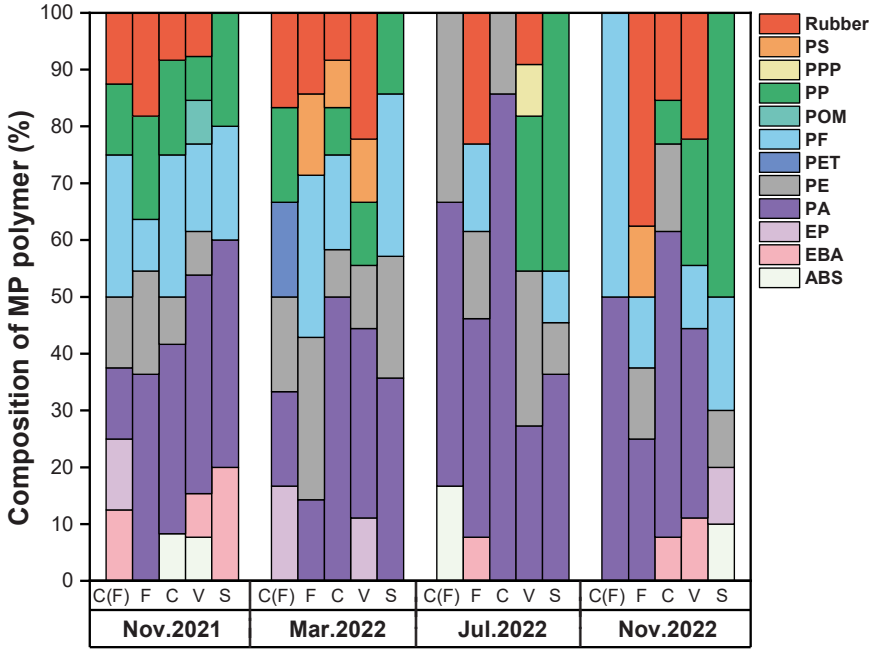

Fig. 4. The composition of microplastic polymer under different land uses and outlet of Jiangou catchment which were sampled in four monitoring periods.

16.18 % of 200–500 μm respectively. It must be noted in this study that MPs accounted for a very small proportion of particle size of 500–5000 μm (Fig. 5).

The typical polymer types in this study were PA, PP and PE. The PA, commonly known as nylon, is often used to produce fertilizer bags, ropes and parts of agricultural machinery. The PP is used as raw material to make plastic woven bags, tapes, ropes and so on [75]. The PE is the main material of mulch film and greenhouse film. The MPs produced by long-term plastic film mulching and greenhouses in the catchment would affect the soil and sediment close to the source and further afield. Many studies suggested that MPs could transport over long distances via the wind which reach up to 800 km [75,78]. In addition, PA, PP and PE are coating materials for producing slow-release fertilizers [68], so applying compound fertilizer and microbial slow-release fertilizers in farmland was an important contributor to PA, PP and PE.

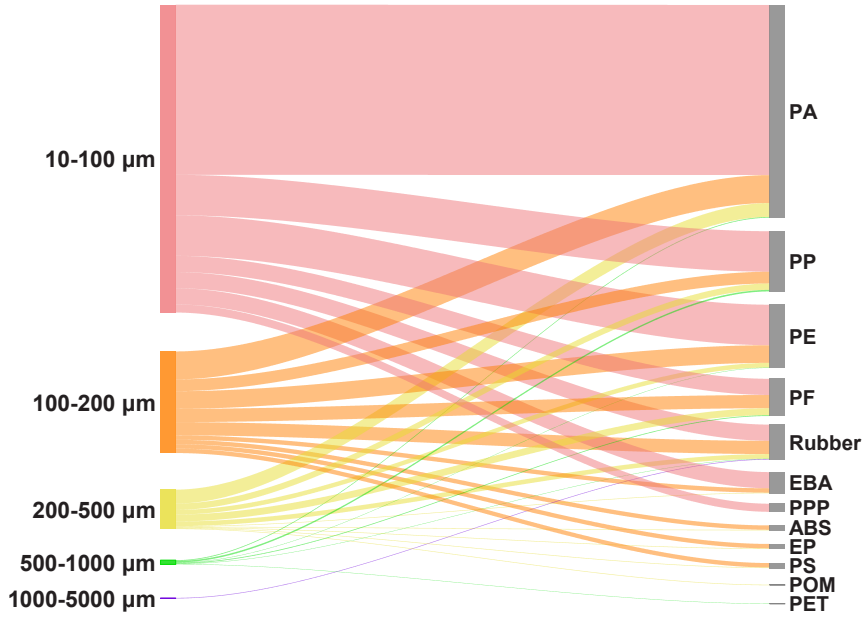

Fig. 5. The corresponding relationship between size and polymer types of MPs.

3.4. ^{7}Be inventory and sedimentation rate

The ^{7}Be inventory of the deposited site in July 2022 was 148.20 ± 8.62 Bq·m^{-2}. This value was larger than the reference site for the same period (77.79 ± 15.68 Bq·m^{-2}), indicating that deposition occurred after the heaviest rainfall (86.3 mm). The catchment sedimentation rate was 68.56 ± 8.40 t·ha^{-1}·event^{-1} in July 2022 (Fig. 6), which was similar to that in previous studies using ^{7}Be tracer technique Esquivel et al. estimated the net erosion of 42.2 ± 3.7 t·ha^{-1} in a steep watershed of Brazil using ^{7}Be technique [79]. The soil erosion in the abandoned farmland slope was 54.5 t·ha^{-1} on average in the northern Loess Plateau of China [80].

3.5. Sediment source contribution and export loads

According to existing literature and our previous study [31], the Bulk δ^{13}C and FAs δ^{13}C (C14:0-C28:0) were regarded as potential tracers, and further statistical tests were conducted to screen suitable tracer

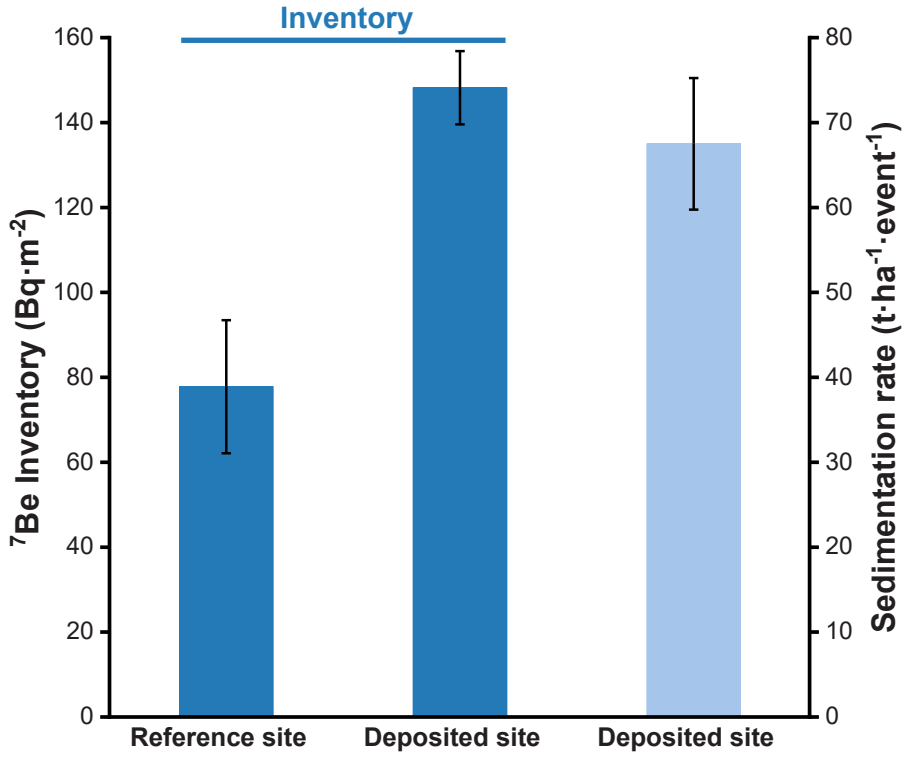

Fig. 6. The ^{7}Be inventory and sedimentation rate in July 2022.

combinations. The isotopic signature was basically similar between F and C(F) (Table S1), which were unlikely to contribute significantly to the mixture of sediment as two separate sources [31,81]. Therefore, forest land (F) and cropland converted from forest (C(F)) were combined to form a new land use classification as F + C(F). The sediment contributors based on vegetation cover were categorized as follows after merging: F + C(F) (forest including cropland converted from forest), C (crop farmland), and V (vegetable farmland).

The boxplots showed the $\delta^{13}C$ values of FAs from C14:0 to C28:0 and Bulk C of different sources and sediment, among which F + C(F) were smaller than those of C and V (more negative). In addition, the $\delta^{13}C$ values of FAs and Bulk C in mixtures fell within the range of the source values except C28:0, which demonstrated that they could be used to discriminate source proportions (Fig. 7). A Kruskal-Wallis test was employed to obtain the level of significance (*P* value) in FAs $\delta^{13}C$ values between all sources. The result of the significance test in the pairwise combinations of all sources (Table 1) showed that the $\delta^{13}C$ values of FAs (C22:0, C24:0 and C26:0) and Bulk C were suitable tracers.

Matrix plots of estimates of each source isotopic proportion demonstrated correlation values between different land uses (Fig. S2). The correlation values between F + C(F) and C as well as between C and V were small, which means that both pairs of land use types exhibited distinct discrimination. Nevertheless, the relatively large correlation value between F + C(F) and V increased the uncertainty. The soil proportions were converted from the resulting isotope proportions of MixSIAR model (Fig. 8). The results indicated that F + C(F) was the dominant sediment source and significantly larger than other land uses in this decreasing order: F + C(F) (50.14 ± 0.27 %) > V (35.74 ± 0.30 %) > C (14.12 ± 0.14 %). The sediment export loads of F + C(F) and V were significantly larger than C. There was no statistically significant difference between F + C(F) and V.

Our study found that F + C(F) was the predominant sediment contributor to the sediment at the outlet of the catchment, which was attributed to the land management policy transition. This transition resulted in the conversion of a large number of forest land into intensive farmland and the construction of massive sprinkler irrigation facilities in the management process. Due to this kind of policy-driven agricultural land management, soil erosion was aggravated and sediment flux increased dramatically in the catchment, which also happened in other countries [82–84]. Consequently, the sediment export loads of F + C(F) and V were statistically significantly larger than those of C, while there was no significant difference between F + C(F) and V. The sediment export loads of V were comparable to F+C(F), which was attributed to the high connectivity with the outlet deposition zone and the increased

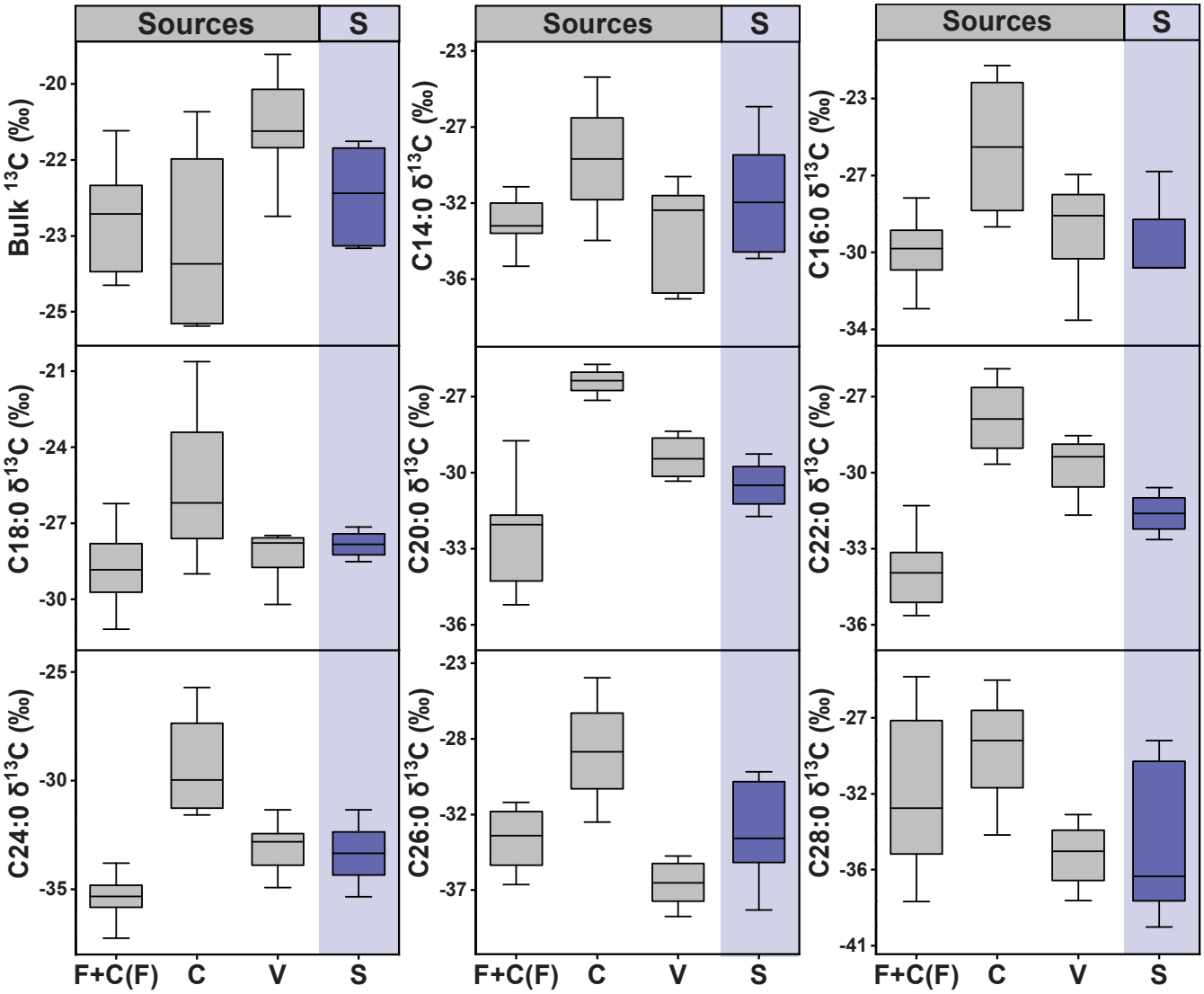

Fig. 7. Range of $\delta^{13}C$ values (‰) of FAs (n-C14:0–n-C28:0) from sources with significantly different tracer values ($p < 0.05$) in July 2022. Note: F + C(F): forest including cropland converted from forest, C: crop farmland, V: vegetable farmland and S: sediments at the outlet of Jiangou catchment.

Table 1
Significance levels derived from Kruskal-Wallis test of $\delta^{13}C$ values of bulk carbon and different FAs for pair wise combinations of land use soil samples.

Land use pairs	Significant levels of $\delta^{13}C$ values								
	Bulk C $\delta^{13}C$	C14:0	C16:0	C18:0	C20:0	C22:0	C24:0	C26:0	C28:0
F + C(F) - C	n.s.	n.s.	*	n.s.	***	****	***	***	n.s.
F + C(F) - V	**	n.s.	n.s.	n.s.	**	****	**	**	n.s.
C - V	*	n.s.	n.s.	n.s.	n.s.	n.s.	n.s.	***	n.s.

Note: F + C(F): forest including cropland converted from forest, C: crop farmland, V: vegetable farmland, non-significant ($p > 0.05$) 'ns';
$p < 0.05$ '*';
$p < 0.01$ '**';
$p < 0.001$ '***';
$p < 0.0001$ '****'.

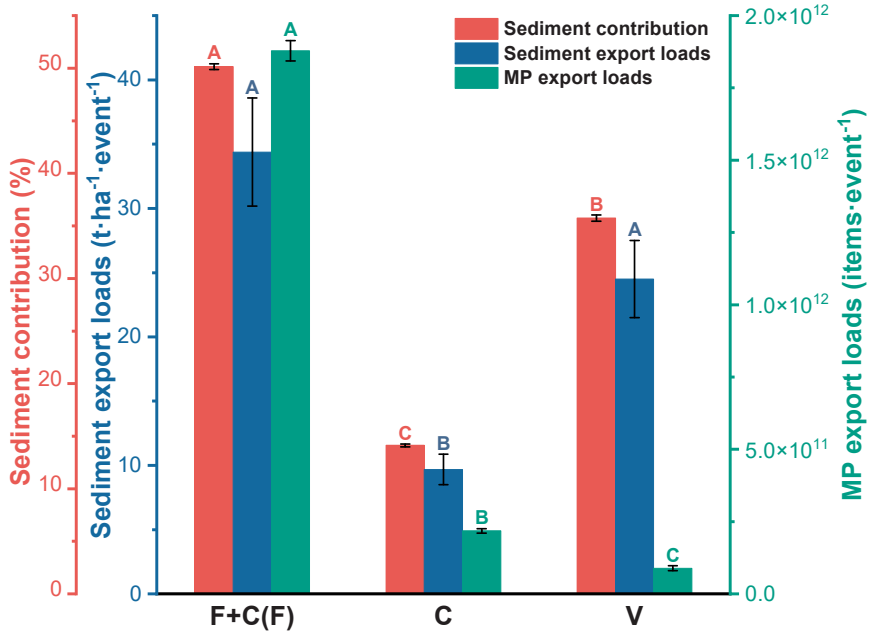

Fig. 8. Relative contribution of different sources to the sediment in the deposition zone and the sediment and microplastic export loads under different land uses in July 2022. Note: Different uppercase letters indicate significant differences in sediment contribution/sediment export loads/microplastic export loads of different sources in July 2022 ($p < 0.05$).

sediment transport due to heavy rainfall event in July 2022 [85].

3.6. Change in microplastic export loads under different land uses

From an ecological perspective, the sediment MPs exported to the water environment would release toxic materials (e.g. POPs and toxic additives) and absorb other pollutants (e.g. heavy metals and antibiotics) that will harm aquatic organisms and pollute drinking water thereby causing environmental risks [4,5,86,87].

Many studies used the pollution loads index method and polymer hazard index method to evaluate the potential ecological risk of soil microplastic pollution [88–91], while our study quantified the microplastic export loads of different land uses to the water environment through soil erosion by field observation at catchment scale. The MPs in sediment were dominantly derived from F+C(F) ($1.88*10^{12} \pm 3.56*10^{10}$ items·event^{-1}), and the least came from C ($2.18*10^{11} \pm 7.82*10^{9}$ items·event^{-1}) and V ($8.88*10^{10} \pm 8.35*10^{9}$ items·event^{-1}). The microplastic export loads of F+C(F) were significantly larger than those of C and V. This implied that F+C(F) is at higher risk of microplastic migration than C and V. The mechanized harvest of wheat followed by sowing with fertilization in July led to soil loosening and decreased anti-scourability of surface soil, which caused a higher risk of soil erosion and MPs loss in F+C(F) [92]. The subsequent flushing effect induced by the extreme rainfall event resulted in the migration of the F+C(F) topsoil with surface runoff. Additionally, the high connectivity between F+C(F) and the mainstreams of the catchment greatly enhanced the transport of sediment and carried MPs after the extreme rainfall event [85].

Interestingly, we found that the sediment export loads of V were statistically significantly larger than those of C, while the microplastic export loads of V were statistically significantly smaller than those of C, which was greatly linked to fertilization. Plastic products were widely used in livestock and poultry breeding, resulting in large amounts of MPs in organic fertilizer (325 ± 511 items·kg^{-1} on average) produced from livestock manure and other waste [93]. Compared with the organic fertilizer, the farmyard chicken manure containing fewer MPs led to a quite low pollution level of microplastic in V. It implied V was at higher risk of sediment contribution compared to C and was supposed to control the soil and water loss.

Monitoring microplastic export loads can provide important information about how much microplastic loads enter water bodies from different sources by soil erosion, especially under the extreme rainfall event, which was critical to guiding the management and mitigation of microplastic pollution in the intensive agricultural catchment. The high level of microplastic abundance of C(F) and the predominant contribution of F+C(F) to sediment greatly increased the microplastic export loads of F+C(F). The maintenance and management of newly-built high-standard farmland slopes after an extreme rainfall event need to be

strengthened to prevent the formation of rill and gully, which would lead to the surface soil MPs entering the water body with runoff.

4. Conclusion

Our study firstly reported the spatio-temporal variability in soil microplastic distribution, including the abundance, size and polymer types, and erosion-induced microplastic export loads under extreme rainfall events in an intensive agricultural catchment (Jiangou catchment) in North China. We have realized all the objectives proposed in the introduction section. The microplastic abundance peaked in November 2022 and varied by land use types, with cropland converted from forest (C(F)) and crop farmland (C) being the highest and vegetable farmland (V) being the lowest on average over a one-year monitoring period. The microplastic abundance in the catchment ranged from 38,223 to 98,602 items•kg^{-1}, with the size of most microplastic particles being below 500 μm. The primary polymer types of microplastic were PA, PP and PE. Furthermore, the microplastic contamination in the catchment was influenced by intensive agricultural activities and rainfall variation. Forest including cropland converted from forest (F+C(F)) was the dominant sediment source and contributed most to the microplastic export loads. The sediment export of V was significantly larger than that of C but its MPs export was significantly smaller than that of C, thus the prevention and control of soil erosion in V is critical. Our study suggested that farmlands which have recently changed land use, due to land management policy shifting, are the hot spot areas to improve fertilizer utilization rate, mitigate soil erosion and carefully dispose of microplastic pollution.

Environmental implication

Microplastics are the hazardous substances in our study, which are emerging pollutants in agricultural non-point source pollution and have adverse impacts on water and soil environments. This study is the first to report the spatio-temporal distribution of soil microplastics, and erosion-induced microplastic export by a novel application of Be-7 and compound specific stable isotope under extreme rainfall events in an intensive agricultural catchment in North China. This study will contribute to evaluating the ecological risks associated with the transfer of microplastics accumulated in the soil to water bodies and help control the microplastic pollution in intensive agricultural catchments.

CRediT authorship contribution statement

Chen Xiaoyan: Writing – review & editing, Writing – original draft, Methodology, Investigation, Formal analysis, Data curation. **Lu Zhaoyang:** Investigation, Data curation. **Heng Lee:** Writing – review & editing. **Chappell Adrian:** Writing – review & editing. **Oshunsanya Suarau Odutola:** Writing – review & editing. **Adu-Gyamfi Joseph:** Writing – review & editing. **Liu Wenxiang:** Writing – review & editing. **Yu Hanqing:** Writing – review & editing, Supervision, Resources, Project administration, Funding acquisition, Conceptualization.

Declaration of Competing Interest

The authors declare that they have no known competing financial interests or personal relationships that could have appeared to influence the work reported in this paper.

Acknowledgement

This work was supported by the Key Technologies Research and Development Program of China (2023YFE0125600) and the International Atomic Energy Agency through coordination research projects (CRP) under Research Contract No. 23008 and technical cooperation project (TCP) RAS 5091. Funding for AC to collaborate on this work was provided by the High-end Foreign Experts Recruitment Program from State of Administration of Foreign Experts Affairs of China.

Appendix A. Supporting information

Supplementary data associated with this article can be found in the online version at doi:10.1016/j.jhazmat.2025.137378.

Data availability

Data will be made available on request.

References

[1] Thompson, R.C., Olsen, Y., Mitchell, R.P., Davis, A., Rowland, S.J., John, A.W.G., et al., 2004. Lost at sea: where is all the plastic? Science 304, 838. https://doi.org/10.1126/science.1094559.
[2] Yuan, Z., Nag, R., Cummins, E., 2022. Human health concerns regarding microplastics in the aquatic environment - from marine to food systems. Sci Total Environ 823, 153730. https://doi.org/10.1016/j.scitotenv.2022.153730.
[3] Jadhav, B., Medyńska-Juraszek, A., 2024. Microplastic and nanoplastic in crops: possible adverse effects to crop production and contaminant transfer in the food chain. Plants 13, 2526. https://doi.org/10.3390/plants13172526.
[4] Owens, P.N., 2020. Soil erosion and sediment dynamics in the anthropocene: a review of human impacts during a period of rapid global environmental change. J Soils Sediment 20, 4115–4143. https://doi.org/10.1007/s11368-020-02815-9.
[5] Shukur, S.A., Hassan, F.M., Fakhry, S.S., Ameen, F., Stephenson, S.L., 2023. Evaluation of microplastic pollution in a lotic ecosystem and its ecological risk. Mar Pollut Bull 194, 115401. https://doi.org/10.1016/j.marpolbul.2023.115401.
[6] Bergmann, M., Wirzberger, V., Krumpen, T., Lorenz, C., Primpke, S., Tekman, M.B., et al., 2017. High quantities of microplastic in arctic deep-sea sediments from the HAUSGARTEN observatory. Environ Sci Technol. https://doi.org/10.1021/acs.est.7b03331.
[7] Horton, A.A., Walton, A., Spurgeon, D.J., Lahive, E., Svendsen, C., 2017. Microplastics in freshwater and terrestrial environments: evaluating the current understanding to identify the knowledge gaps and future research priorities. Sci Total Environ 586, 127–141. https://doi.org/10.1016/j.scitotenv.2017.01.190.
[8] Li, Y., Wu, M., Li, H., Xue, H., Tao, J., Li, M., et al., 2023. Current advances in microplastic contamination in aquatic sediment: analytical methods, global occurrence, and effects on elemental cycling. TrAC Trends Anal Chem 168, 117331. https://doi.org/10.1016/j.trac.2023.117331.
[9] Hu, D., Zhang, C., Ma, B., Liu, Z., Yang, X., Yang, L., 2020. The characteristics of rainfall runoff pollution and its driving factors in Northwest semiarid region of China - a case study of Xi'an. Sci Total Environ 726, 138384. https://doi.org/10.1016/j.scitotenv.2020.138384.
[10] Yang, L., Li, J., Zhou, K., Feng, P., Dong, L., 2021. The effects of surface pollution on urban river water quality under rainfall events in Wuqing district, Tianjin, China. J Clean Prod 293, 126136. https://doi.org/10.1016/j.jclepro.2021.126136.
[11] He, L., Ou, Z., Fan, J., Zeng, B., Guan, W., 2022. Research on the non-point source pollution of microplastics. Front Chem 10. https://doi.org/10.3389/fchem.2022.956547.
[12] Silori, R., Shrivastava, V., Mazumder, P., Mootapally, C., Pandey, A., Kumar, M., 2023. Understanding the underestimated: Occurrence, distribution, and interactions of microplastics in the sediment and soil of China, India, and Japan. Environ Pollut 320, 120978. https://doi.org/10.1016/j.envpol.2022.120978.
[13] Zarnaghsh, A., Husic, A., 2021. Degree of anthropogenic land disturbance controls fluvial sediment hysteresis. Environ Sci Technol 55, 13737–13748. https://doi.org/10.1021/acs.est.1c00740.
[14] Liu, L., Wang, Z., Ye, Y., Qi, K., 2023. Effects of agricultural land types on microplastic abundance: a nationwide meta-analysis in China. Sci Total Environ 892. https://doi.org/10.1016/j.scitotenv.2023.164400.
[15] Tian, L., Jinjin, C., Ji, R., Ma, Y., Yu, X., 2022. Microplastics in agricultural soils: sources, effects, and their fate. Curr Opin Environ Sci Health 25, 100311. https://doi.org/10.1016/j.coesh.2021.100311.
[16] Corradini, F., Casado, F., Leiva, V., Huerta-Lwanga, E., Geissen, V., 2021. Microplastics occurrence and frequency in soils under different land uses on a regional scale. Sci Total Environ 752, 141917. https://doi.org/10.1016/j.scitotenv.2020.141917.
[17] Zhang, J., Li, Z., Zhou, X., Ding, W., Wang, X., Zhao, M., et al., 2023. Long-term application of organic compost is the primary contributor to microplastic pollution of soils in a wheat-maize rotation. Sci Total Environ 866, 161123. https://doi.org/10.1016/j.scitotenv.2022.161123.
[18] Zhang, Y., Wang, K., Chen, Weizhi, Ba, Y., Khan, K., Chen, Wei, et al., 2022. Effects of land use and landscape on the occurrence and distribution of microplastics in soil, China. Sci Total Environ 847, 157598. https://doi.org/10.1016/j.scitotenv.2022.157598.
[19] Yu, L., Zhang, J., Liu, Y., Chen, L., Tao, S., Liu, W., 2021. Distribution characteristics of microplastics in agricultural soils from the largest vegetable production base in China. Sci Total Environ 756. https://doi.org/10.1016/j.scitotenv.2020.143860.

[20] Wang, Y., Jing, S., Hou, P., Ni, R., Niu, L., Wanger, T.C., et al., 2024. Soil erosion is a major drive for nano & micro-plastics to enter riverine systems from cultivated land. Water Res 256, 121597. https://doi.org/10.1016/j.watres.2024.121597.
[21] Hurley, R.R., Nizzetto, L., 2018. Fate and occurrence of micro(nano)plastics in soils: Knowledge gaps and possible risks. Curr. Opin. Environ. Sci. Health, Micro and Nanoplastics Edited by Dr. Teresa A.P. Rocha-Santos 1, 6–11. https://doi.org/10.1016/j.coesh.2017.10.006.
[22] Yu, H., Zhang, W., Zheng, L., Li, T., Hai, C., Wang, Y., et al., 2024. A review of the migration mechanisms of microplastics in terrestrial environments. Environ Eng Res 29. https://doi.org/10.4491/eer.2023.734.
[23] Collins, A.L., Blackwell, M., Boeckx, P., Chivers, C.-A., Emelko, M., Evrard, O., et al., 2020. Sediment source fingerprinting: benchmarking recent outputs, remaining challenges and emerging themes. J Soils Sediment 20, 4160–4193. https://doi.org/10.1007/s11368-020-02755-4.
[24] Mabit, L., Gibbs, M., Mbaye, M., Meusburger, K., Toloza, A., Resch, C., et al., 2018. Novel application of compound specific stable isotope (CSSI) techniques to investigate on-site sediment origins across arable fields. Geoderma 316, 19–26. https://doi.org/10.1016/j.geoderma.2017.12.008.
[25] García-Comendador, J., Martínez-Carreras, N., Fortesa, J., Borràs, A., Calsamiglia, A., Estrany, J., 2020. Analysis of post-fire suspended sediment sources by using colour parameters. Geoderma 379, 114638. https://doi.org/10.1016/j.geoderma.2020.114638.
[26] Das, A., Remesan, R., Collins, A.L., Gupta, A.K., 2023. The spatio-temporal dynamics of suspended sediment sources based on a novel indexing approach combining Bayesian geochemical fingerprinting with physically-based modelling. J Environ Manag 345, 118649. https://doi.org/10.1016/j.jenvman.2023.118649.
[27] de Rosas, J.P., Esquivel, A.D., Martinez Heimann, D., Negri, A.E., Lohaiza, F., Valladares, D.L., et al., 2018. Using beryllium-7 to evaluate soil erosion processes in agricultural lands in semiarid regions of Central Argentina. Environ Earth Sci 77, 587. https://doi.org/10.1007/s12665-018-7767-x.
[28] Bravo-Linares, C., Schuller, P., Castillo, A., Ovando-Fuentealba, L., Muñoz-Arcos, E., Alarcón, O., et al., 2018. First use of a compound-specific stable isotope (CSSI) technique to trace sediment transport in upland forest catchments of Chile. Sci Total Environ 618, 1114–1124. https://doi.org/10.1016/j.scitotenv.2017.09.163.
[29] Hirave, P., Nelson, D.B., Glendell, M., Alewell, C., 2023. Land-use-based freshwater sediment source fingerprinting using hydrogen isotope compositions of long-chain fatty acids. Sci Total Environ 875, 162638. https://doi.org/10.1016/j.scitotenv.2023.162638.
[30] Yu, H., Adu-Gyamfi, J., Oshunsanya, S.O., Chappell, A., Liu, W., Zheng, Y., et al., 2023. Novel sediment source fingerprinting quantifying erosion-induced total nitrogen and total phosphorus outputs from an intensive agricultural catchment, North China. Int Soil Water Conserv Res 11, 494–506. https://doi.org/10.1016/j.iswcr.2022.10.006.
[31] Lu, Z., Yu, H., Adu-Gyamfi, J., Wang, H., Chappell, A., Oshunsanya, S.O., et al., 2024. Land management policy shift influenced seasonal variation of erosion-induced nitrogen and phosphorus outputs from intensive agricultural catchment. Sci Total Environ 918, 170590. https://doi.org/10.1016/j.scitotenv.2024.170590.
[32] NDRC, 2021. National High-standard Farmland Construction Plan (2021-2030). ⟨https://www.ndrc.gov.cn/fggz/fzzlgh/gjjzxgh/202111/t20211102_1302810.html⟩ (accessed 11.15.23).
[33] MARA, 2023. Shunyi District high standard farmland area will reach 159.5 km^2. ⟨http://www.moa.gov.cn/xw/qg/202301/t20230120_6419195.htm⟩ (accessed 11.14.23).
[34] Brandt, C., Cadisch, G., Nguyen, L.T., Vien, T.D., Rasche, F., 2016. Compound-specific δ13C isotopes and Bayesian inference for erosion estimates under different land use in Vietnam. Geoderma Reg 7, 311–322. https://doi.org/10.1016/j.geodrs.2016.06.001.
[35] Ling, Q., Yang, B., Jiao, J., Ma, X., Zhao, W., Zhang, X., 2023. Response of microplastic occurrence and migration to heavy rainstorm in agricultural catchment on the Loess plateau. J Hazard Mater 460, 132416. https://doi.org/10.1016/j.jhazmat.2023.132416.
[36] Zhang, H., Huang, Y., An, S., Zhao, J., Xiao, L., Li, H., et al., 2022. Microplastics trapped in soil aggregates of different land-use types: a case study of Loess Plateau terraces, China. Environ Pollut 310, 119880. https://doi.org/10.1016/j.envpol.2022.119880.
[37] Mabit, L., Blake, W. (Eds.), 2019. Assessing Recent Soil Erosion Rates through the Use of Beryllium-7 (Be-7). Springer International Publishing, Cham. https://doi.org/10.1007/978-3-030-10982-0.
[38] Li, J., Zhu, B., Huang, B., Ma, J., Lu, C., Chi, G., et al., 2023. Vertical distribution and characteristics of soil microplastics under different land use patterns: a case study of Shouguang City, China. Sci Total Environ 903, 166154. https://doi.org/10.1016/j.scitotenv.2023.166154.
[39] Oßmann, B.E., Sarau, G., Holtmannspötter, H., Pischetsrieder, M., Christiansen, S. H., Dicke, W., 2018. Small-sized microplastics and pigmented particles in bottled mineral water. Water Res 141, 307–316. https://doi.org/10.1016/j.watres.2018.05.027.
[40] Li, J., Zhang, J., Ren, S., Huang, D., Liu, F., Li, Z., et al., 2023. Atmospheric deposition of microplastics in a rural region of North China Plain. Sci Total Environ. https://doi.org/10.1016/j.scitotenv.2023.162947.
[41] Huppertsberg, S., Knepper, T.P., 2018. Instrumental analysis of microplastics—benefits and challenges. Anal Bioanal Chem 410, 6343–6352. https://doi.org/10.1007/s00216-018-1210-8.
[42] Xia, F., Liu, H., Zhang, J., Wang, D., 2022. Migration characteristics of microplastics based on source-sink investigation in a typical urban wetland. Water Res. https://doi.org/10.1016/j.watres.2022.118154.
[43] Hu, W., Tang, R., Yuan, S., Gong, M., Shi, P., Wang, W., et al., 2023. Modification of fluorescence staining method for small-sized microplastic quantification: focus on the interference exclusion and exposure time optimization. Environ Sci Pollut Res 30, 56330–56342. https://doi.org/10.1007/s11356-023-26226-8.
[44] Tong, H., Jiang, Q., Hu, X., Zhong, X., 2020. Occurrence and identification of microplastics in tap water from China. Chemosphere 252, 126493. https://doi.org/10.1016/j.chemosphere.2020.126493.
[45] Bai, R., Fan, R., Xie, C., Liu, Qin, Liu, Qi, Yan, C., et al., 2023. Microplastics are overestimated due to poor quality control of reagents. J Hazard Mater 459, 132068. https://doi.org/10.1016/j.jhazmat.2023.132068.
[46] Prarat, P., Hongsawat, P., Chouychai, B., 2024. Microplastic occurrence in surface sediments from coastal mangroves in Eastern Thailand: abundance, characteristics, and ecological risk implications. Reg Stud Mar Sci 71, 103389. https://doi.org/10.1016/j.rsma.2024.103389.
[47] Bai, R., Liu, H., Cui, J., Wu, Y., Guo, X., Liu, Qin, et al., 2024. The characteristics and influencing factors of farmland soil microplastic in Hetao Irrigation District, China. J Hazard Mater 465, 133472. https://doi.org/10.1016/j.jhazmat.2024.133472.
[48] Li, M., Xu, X., Wang, J., Deng, L., Wu, Z., Yang, D., et al., 2024. Complex microplastics significantly influence the assembly process of lake bacterial communities. J Hazard Mater 480, 135867. https://doi.org/10.1016/j.jhazmat.2024.135867.
[49] Gibbs, M., 2014. Protocols on the use of compound-specific stable isotopes to identify and apportion soil sources from land use. ⟨http://www-naweb.iaea.org/nafa/swmn/public/CSSI-technique-protocols-revised-2013.pdf⟩ (accessed 11.7.23).
[50] Gibbs, M., Leduc, D., Nodder, S.D., Kingston, A., Swales, A., Rowden, A.A., et al., 2020. Novel application of a compound-specific stable isotope (CSSI) tracking technique demonstrates connectivity between terrestrial and deep-sea ecosystems via submarine canyons. Front Mar Sci 7. https://doi.org/10.3389/fmars.2020.00608.
[51] Yu, H., Li, Y., Oshunsanya, S.O., Are, K.S., Geng, Y., Saggar, S., et al., 2019. Re-introduction of light grazing reduces soil erosion and soil respiration in a converted grassland on the Loess Plateau, China. Agric Ecosyst Environ 280, 43–52. https://doi.org/10.1016/j.agee.2019.04.020.
[52] Kieta, K.A., Owens, P.N., Petticrew, E.L., 2024. Evaluating and improving the assessment of compound-specific stable isotope derived sediment fingerprinting results in an agricultural watershed in British Columbia, Canada. CATENA 246, 108351. https://doi.org/10.1016/j.catena.2024.108351.
[53] Reiffarth, D.G., Petticrew, E.L., Owens, P.N., Lobb, D.A., 2016. Sources of variability in fatty acid (FA) biomarkers in the application of compound-specific stable isotopes (CSSIs) to soil and sediment fingerprinting and tracing: a review. Sci Total Environ 565, 8–27. https://doi.org/10.1016/j.scitotenv.2016.04.137.
[54] Parnell, A.C., Phillips, D.L., Bearhop, S., Semmens, B.X., Ward, E.J., Moore, J.W., et al., 2013. Bayesian stable isotope mixing models. Environmetrics 24, 387–399. https://doi.org/10.1002/env.2221.
[55] Stock., B., Jackson., A., Ward., E., Jason.,V., 2018. MixSIAR GUI User Manual, Version 3.1.9. ⟨https://github.com/brianstock/MixSIAR⟩. https://doi.org/10.5281/zenodo.1209993 (accessed 11.27.23).
[56] Upadhayay, H.R., Zhang, Y., Granger, S.J., Micale, M., Collins, A.L., 2022. Prolonged heavy rainfall and land use drive catchment sediment source dynamics: appraisal using multiple biotracers. Water Res 216, 118348. https://doi.org/10.1016/j.watres.2022.118348.
[57] Walling, D.E., He, Q., Blake, W., 1999. Use of 7 Be and 137 Cs measurements to document short- and medium-term rates of water-induced soil erosion on agricultural land. Water Resour Res 35, 3865–3874. https://doi.org/10.1029/1999WR900242.
[58] Yuan, B., Gan, W., Sun, J., Lin, B., Chen, Z., 2023. Depth profiles of microplastics in sediments from inland water to coast and their influential factors. Sci Total Environ 903, 166151. https://doi.org/10.1016/j.scitotenv.2023.166151.
[59] Yu, Y., Zhang, Z., Zhang, Y., Jia, H., Li, Y., Yao, H., 2023. Abundances of agricultural microplastics and their contribution to the soil organic carbon pool in plastic film mulching fields of Xinjiang, China. Chemosphere 316. https://doi.org/10.1016/j.chemosphere.2023.137837.
[60] Huang, B., Sun, L., Liu, M., Huang, H., He, H., Han, F., et al., 2021. Abundance and distribution characteristics of microplastic in plateau cultivated land of Yunnan Province, China. Environ Sci Pollut Res 28, 1675–1688. https://doi.org/10.1007/s11356-020-10527-3.
[61] Zhang, G.S., Liu, Y.F., 2018. The distribution of microplastics in soil aggregate fractions in southwestern China. Sci Total Environ 642, 12–20. https://doi.org/10.1016/j.scitotenv.2018.06.004.
[62] Liu, M., Lu, S., Song, Y., Lei, L., Hu, J., Lv, W., et al., 2018. Microplastic and mesoplastic pollution in farmland soils in suburbs of Shanghai, China. Environ Pollut 242, 855–862. https://doi.org/10.1016/j.envpol.2018.07.051.
[63] Ya, H., Jiang, B., Xing, Y., Zhang, T., Lv, M., Wang, X., 2021. Recent advances on ecological effects of microplastics on soil environment. Sci Total Environ 798. https://doi.org/10.1016/j.scitotenv.2021.149338.
[64] Zhang, S., Wang, W., Yan, P., Wang, J., Yan, S., Liu, X., et al., 2023. Microplastic migration and distribution in the terrestrial and aquatic environments: a threat to biotic safety. J Environ Manag 333, 117412. https://doi.org/10.1016/j.jenvman.2023.117412.
[65] Zhou, Y., Liu, X., Wang, J., 2019. Characterization of microplastics and the association of heavy metals with microplastics in suburban soil of central China. Sci Total Environ 694, 133798. https://doi.org/10.1016/j.scitotenv.2019.133798.
[66] Zhang, Y., Peng, Y., Xu, S., Zhang, S., Zhou, G., Yang, J., et al., 2022. Distribution characteristics of microplastics in urban rivers in Chengdu city: the influence of

land-use type and population and related suggestions. Sci Total Environ 846, 157411. https://doi.org/10.1016/j.scitotenv.2022.157411.
[67] Cao, L., Wu, D., Liu, P., Hu, W., Xu, L., Sun, Y., et al., 2021. Occurrence, distribution and affecting factors of microplastics in agricultural soils along the lower reaches of Yangtze River, China. Sci Total Environ 794, 148694. https://doi.org/10.1016/j.scitotenv.2021.148694.
[68] Kassem, I., Ablouh, E.-H., Bouchtaoui, F.-Z.E., Jaouahar, M., Achaby, M.E., 2024. Polymer coated slow/ controlled release granular fertilizers: fundamentals and research trends. Prog Mater Sci 144, 101269. https://doi.org/10.1016/j.pmatsci.2024.101269.
[69] Katsumi, N., Kusube, T., Nagao, S., Okochi, H., 2021. Accumulation of microcapsules derived from coated fertilizer in paddy fields. Chemosphere 267, 129185. https://doi.org/10.1016/j.chemosphere.2020.129185.
[70] Zhao, S., Zhang, Z., Chen, L., Cui, Q., Cui, Y., Song, D., et al., 2022. Review on migration, transformation and ecological impacts of microplastics in soil. Appl Soil Ecol 176, 104486. https://doi.org/10.1016/j.apsoil.2022.104486.
[71] Zhang, S., Liu, X., Hao, X., Wang, J., Zhang, Y., 2019. Distribution of low-density microplastics in the Mollisol farmlands of northeast China. Sci Total Environ 708, 135091. https://doi.org/10.1016/j.scitotenv.2019.135091.
[72] Xia, F., Tan, Q., Qin, H., Wang, D., Cai, Y., Zhang, J., 2023. Sequestration and export of microplastics in urban river sediments. Environ Int 181, 108265. https://doi.org/10.1016/j.envint.2023.108265.
[73] Drummond, J.D., Nel, H.A., Packman, A.I., Krause, S., 2020. Significance of hyporheic exchange for predicting microplastic fate in rivers. Environ Sci Technol Lett 7, 727–732. https://doi.org/10.1021/acs.estlett.0c00595.
[74] Zhao, W., Li, J., Liu, M., Wang, R., Zhang, B., Meng, X.-Z., et al., 2024. Seasonal variations of microplastics in surface water and sediment in an inland river drinking water source in southern China. Sci Total Environ 908, 168241. https://doi.org/10.1016/j.scitotenv.2023.168241.
[75] Zhang, H., Huang, Y., An, S., Li, H., Deng, X., Wang, P., et al., 2022. Land-use patterns determine the distribution of soil microplastics in typical agricultural areas on the eastern Qinghai-Tibetan Plateau. J Hazard Mater 426, 127806. https://doi.org/10.1016/j.jhazmat.2021.127806.
[76] Lv, M., Jiang, B., Xing, Y., Ya, H., Zhang, T., Wang, X., 2022. Recent advances in the breakdown of microplastics: strategies and future prospectives. Environ Sci Pollut Res 29, 65887–65903. https://doi.org/10.1007/s11356-022-22004-0.
[77] Zhang, S., Wang, J., Hao, X., 2020. Fertilization accelerates the decomposition of microplastics in mollisols. Sci Total Environ 722, 137950. https://doi.org/10.1016/j.scitotenv.2020.137950.
[78] Dong, H., Wang, L., Wang, X., Xu, L., Chen, M., Gong, P., et al., 2021. Microplastics in a remote lake basin of the tibetan plateau: impacts of atmospheric transport and glacial melting. Environ Sci Technol 55, 12951–12960. https://doi.org/10.1021/acs.est.1c03227.
[79] Esquivel, A.D., Moreira, R.M., Monteiro, R.P.G., Rochido Dos Santos, A.A., Valladares, D.L., Juri Ayub, J., 2021. Quantification of soil erosion using 7Be in a steep watershed used for natural grazing in Brazil. Isot Environ Health Stud 57, 316–331. https://doi.org/10.1080/10256016.2021.1918687.
[80] Li, X., Zhang, F., He, Q., Yang, M., 2023. Correspondence analysis between vegetation cover and sheet erosion rate on an abandoned farmland slope based on 7Be measurement. CATENA 222, 106886. https://doi.org/10.1016/j.catena.2022.106886.
[81] Swales, A., Gibbs, M.M., 2020. Transition in the isotopic signatures of fatty-acid soil biomarkers under changing land use: insights from a multi-decadal chronosequence. Sci Total Environ 722, 137850. https://doi.org/10.1016/j.scitotenv.2020.137850.
[82] Daniel, D.W., Smith, L.M., McMurry, S.T., 2015. Land use effects on sedimentation and water storage volume in playas of the rainwater basin of Nebraska. Land Use Policy 42, 426–431. https://doi.org/10.1016/j.landusepol.2014.08.013.
[83] Starr, S.M., Heintzman, L.J., Mulligan, K.R., Barbato, L.S., McIntyre, N.E., 2016. Using remotely sensed imagery to document how land use drives turbidity of playa waters in Texas. Remote Sens 8. https://doi.org/10.3390/rs8030192.
[84] Zhou, M., Deng, J., Lin, Y., Zhang, L., He, S., Yang, W., 2021. Evaluating combined effects of socio-economic development and ecological conservation policies on sediment retention service in the Qiantang River Basin, China. J Clean Prod 286. https://doi.org/10.1016/j.jclepro.2020.124961.
[85] Koci, J., Sidle, R.C., Jarihani, B., Cashman, M.J., 2020. Linking hydrological connectivity to gully erosion in savanna rangelands tributary to the Great Barrier Reef using structure-from-motion photogrammetry. Land Degrad Dev 31, 20–36. https://doi.org/10.1002/ldr.3421.
[86] Yu, Y., Kumar, M., Bolan, S., Padhye, L.P., Bolan, N., Li, S., et al., 2024. Various additive release from microplastics and their toxicity in aquatic environments. Environ Pollut 343, 123219. https://doi.org/10.1016/j.envpol.2023.123219.
[87] Rafa, N., Ahmed, B., Zohora, F., Bakya, J., Ahmed, S., Ahmed, S.F., et al., 2024. Microplastics as carriers of toxic pollutants: Source, transport, and toxicological effects. Environ Pollut 343, 123190. https://doi.org/10.1016/j.envpol.2023.123190.
[88] Qiu, Y., Zhou, S., Zhang, C., Qin, W., Lv, C., 2023. A framework for systematic microplastic ecological risk assessment at a national scale. Environ Pollut 327, 121631. https://doi.org/10.1016/j.envpol.2023.121631.
[89] Kabir, A.H.M.E., Sekine, M., Imai, T., Yamamoto, K., Kanno, A., Higuchi, T., 2021. Assessing small-scale freshwater microplastics pollution, land-use, source-to-sink conduits, and pollution risks: perspectives from Japanese rivers polluted with microplastics. Sci Total Environ 768, 144655. https://doi.org/10.1016/j.scitotenv.2020.144655.
[90] Wan, S., Xu, G., Xiong, P., Qiao, H., Chen, X., Gu, L., et al., 2024. Microplastic pollution characteristics and ecological risk assessment in the Wuding River Basin, China. Environ Pollut 356, 124228. https://doi.org/10.1016/j.envpol.2024.124228.
[91] Xu, P., Peng, G., Su, L., Gao, Y., Gao, L., Li, D., 2018. Microplastic risk assessment in surface waters: a case study in the Changjiang Estuary, China. Mar Pollut Bull 133, 647–654. https://doi.org/10.1016/j.marpolbul.2018.06.020.
[92] Bogunovic, I., Pereira, P., Kisic, I., Sajko, K., Sraka, M., 2018. Tillage management impacts on soil compaction, erosion and crop yield in Stagnosols (Croatia). CATENA 160, 376–384. https://doi.org/10.1016/j.catena.2017.10.009.
[93] Zhang, S., Li, Y., Chen, X., Jiang, X., Li, J., Yang, L., et al., 2022. Occurrence and distribution of microplastics in organic fertilizers in China. Sci Total Environ 844, 157061. https://doi.org/10.1016/j.scitotenv.2022.157061.